Remediation Ecology
https://www.sciltp.com/journals/re

Article

Transforming Sediment from Nutrient Source to Sink through Electrokinetic Geosynthetics-Driven Porewater Drainage

Xianqiang Tang [1,2,3,*], Rui Li [1,2,3], Yanping Hu [1,2,3], Danyang Wang [1,2,3], Junjun Gu [1,2,3] and Zhenhua Wang [1,2,3]

[1] Basin Water Environmental Research Department, Changjiang River Scientific Research Institute, Wuhan 430010, China
[2] Key Lab of Basin Water Resource and Eco-Environmental Science in Hubei Province, Wuhan 430010, China
[3] Hubei Provincial Field Scientific Observation and Research Station for Eco-environmental Effects of the Danjiangkou Water Diversion Project, Shiyan 442000, China
* Correspondence: ckyshj@126.com

How To Cite: Tang, X.; Li, R.; Hu, Y.; et al. Transforming Sediment from Nutrient Source to Sink through Electrokinetic Geosynthetics-Driven Porewater Drainage. *Remediation Ecology* **2026**, *1* (1), 2.

Received: 4 August 2025
Revised: 22 September 2025
Accepted: 31 December 2025
Published: 12 January 2026

Abstract: Porewater, a key reservoir of nutrients, plays a critical role in sediment nutrient release. This study used electrokinetic geosynthetics (EKGs) as electrodes to drain sediment porewater in the presence of 20 cm-deep overlying water and conducted five sets of indoor experiments (one control group and four groups exposed to voltage gradients of 0, 0.5 (intermittent power IP), 0.5 (continuous power CP), 1.0 V/cm (IP)) to investigate the performance and mechanisms of porewater drainage regulating sediment nutrient release and the response of microbial communities. Total nitrogen (TN) release flux dramatically decreased to ≤10% of its maximum within 14 days, while total phosphorus (TP) release flux clearly decreased after fluctuating for nearly 28 days. 0.5 and 1.0 V/cm were more effective for restraining TN and TP release, respectively. For both nitrogen and phosphorus, the drainage of porewater changed the sediment's role from nutrient source to sink, effectively restraining nutrient accumulation in the overlying water. Physical processes including porewater renewal by overlying water, gravity drainage, and sediment pore compression were the key mechanisms restricting sediment nutrient release, while electromigration and electrochemical oxidation promoted nutrient transformation and separation. The drainage caused a non-significant decline in community abundance indices but not changed the dominant species of the sediment microorganisms.

Keywords: electrokinetic geosynthetics; eutrophication; nitrogen; nutrient; phosphorus; sediment remediation

1. Introduction

Eutrophication in waterbodies such as rivers and lakes has been a long-standing environmental issue worldwide [1]. When the external pollution load is controlled, the internal release of nutrients (mainly nitrogen and phosphorus) from underlying sediment becomes the main cause of eutrophication [2]. Nitrogen and phosphorus are released at the sediment-water interface, primarily originating from porewater and sediment fractions with high mobility, such as weakly adsorbed phosphorus and ion-exchangeable nitrogen [3]. Sediment nitrogen and phosphorus first migrate into porewater through a series of processes including ion exchange, mineralization, and gradient diffusion and then move into overlying water through sediment-water interface under the influence of concentration gradient [4].

As the transfer station for sediment nutrients release into overlying water, porewater is characterized by rich content (accounting for 40–60% volume of 0–30 cm surface sediment) and high load of dissolved nutrients (nitrogen and phosphorus concentrations in porewater are 5–30 times higher than those in overlying water) [5]. Porewater is the source of nutrients relative to overlying water, and the sink of nutrients relative to bottom sediment. Abundant movable nutrients in sediment porewater result in eutrophication and algal blooms [6]. To address this, various technologies (e.g., environmental dredging, active material covering, aquatic plant cultivation, and sediment aeration) have been used to reduce the content of sediment nutrients as well as to restrain its release [7,8].

Environmental dredging directly removes polluted sediment. The high-water content and complex pollutant components of dredged slurry however result in costly dehydration and purification [5]. In-situ capping with active materials restrains nutrients release through reducing the chemical activity of porewater nutrients, but it could not remove nutrients and the efficiency of in-situ capping decreases with time [9]. Aquatic plants can assimilate porewater nutrients but their requirement for growth is very strict (e.g., water depth and turbidity), and rotten plant tissues may contribute to eutrophication if poorly managed [10].

Electrokinetic remediation exhibits great potential to cover the shortages of the above technologies [11,12]. Electrokinetic remediation includes various processes such as electromigration, electrophoresis, electroosmotic flow, and oxidation-reduction reactions. Among which electromigration is the main driving force for the separation of pollutants and is influenced by many factors such as current density, pollutant content, sediment composition, porewater pH, and conductivity [13]. Previous studies have found that electrokinetic remediation is effective for removing nitrogen and phosphorus from various environmental medium such as slag, groundwater, soil, sediment, and sludge [14–18].

The effectiveness of electrokinetic remediation mainly lies in the process of porewater drainage which in-situ reduces the load and release flux of sediment nutrients [19]. Electrokinetic geosynthetics (EKGs) that works as electrodes is the key material for porewater drainage [20]. Porewater drainage through EKG changes the physical structure (e.g., porosity) and chemical characteristics (e.g., pH values, redox potential, and oxygen content) of surface sediment and affects sediment microbial communities (e.g., species abundance and diversity), thereby regulating the release flux of sediment nutrients and the stoichiometric features of nutrients in the overlying water. However, previous studies mainly focused on the performance of porewater drainage and sediment nutrient reduction [19–21], little is known about the mechanisms underlying the migration of nutrients in overlying water, porewater, and sediment particles.

In this study, EKGs were used as electrodes to perform electrokinetic remediation experiment on samples of eutrophic sediments and overlying water. The aims of the paper were to (i) assess the performance of porewater drainage on the release of sediment nitrogen and phosphorus; (ii) elucidate the physio-chemical processes control the performance; and (iii) investigate the response of sediment microbial communities to porewater drainage. The study elucidated the synergistic interaction between physical processes and electrochemical processes during EKG-driven porewater drainage, and quantitatively assessed their contribution to the transformation of sediment source-sink functions.

2. Materials and Methods

2.1. Experimental Design and Procedure

The electrokinetic remediation experimental apparatus consisted of three parts, i.e., porewater drainage unit, peristaltic pump, and direct current (DC) power supply. The patent-designed porewater drainage unit extracts sediment porewater through overlying water [19]. The porewater drainage unit has a three-layer sandwich structure (Figure 1). The innermost layer is an EKG with vertical drainage grooves, serving as an electrode. The middle layer is an organic glass plate with evenly distributed holes, used to fix the EKG and permit the porewater to freely enter into the vertical drainage grooves. The outermost layer is a cotton filter cloth to prevent the invasion of sediment particles and the clogging of the EKG. When a DC electric field (30 V) is applied, movable sediment nutrients migrate to the EKG and are then separated through porewater drainage by the peristaltic pump. As the porewater is drained, the nutrients in the overlying water, porewater, and sediment particles are continuously dialyzed and drained.

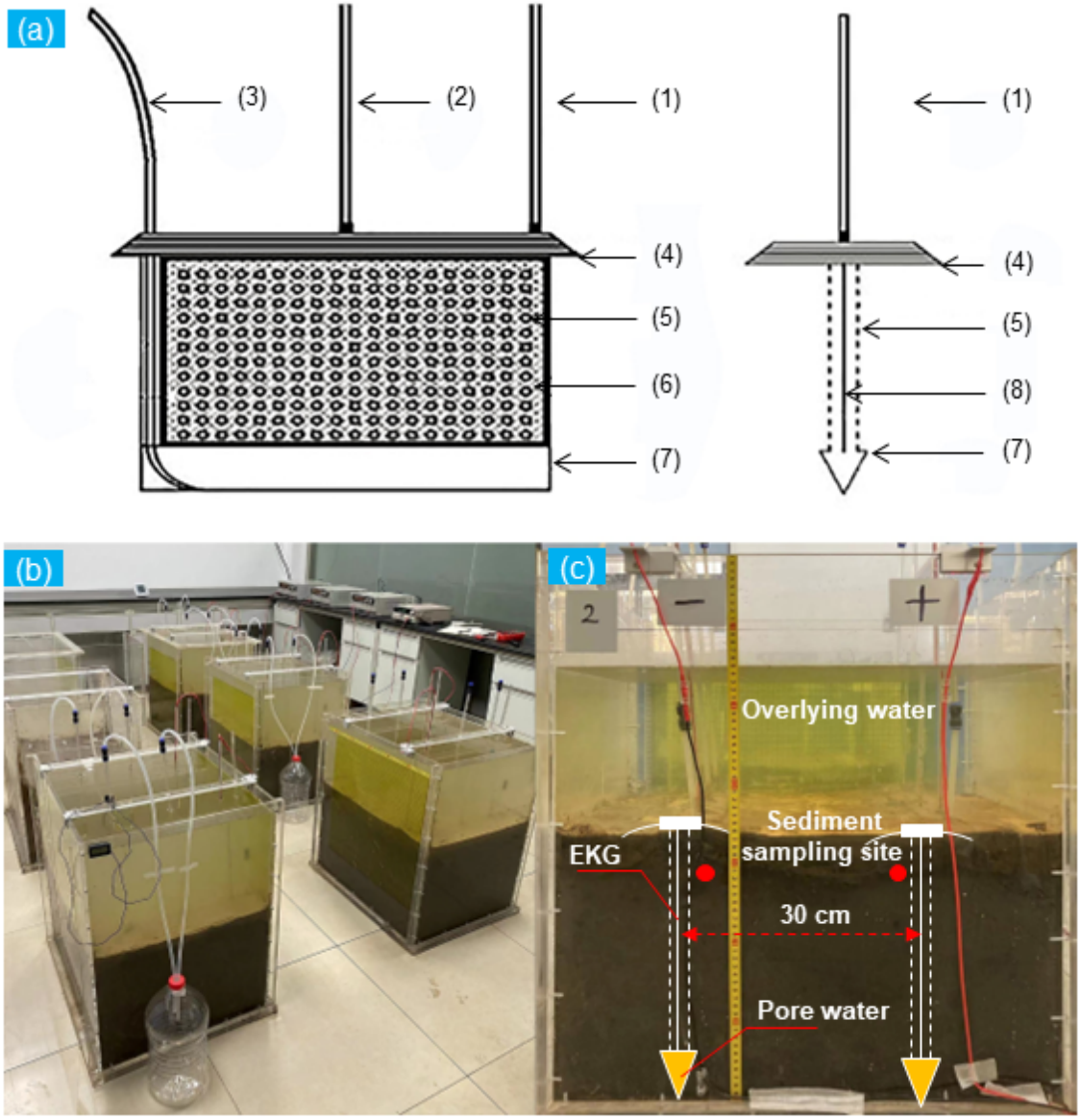

Figure 1. (**a**) Schematic of porewater drainage unit; (**b**) indoor experimental setting; and (**c**) schematic of EKR experiment. (1) Waterproof wire; (2) vent tube; (3) porewater drainage tube; (4) overlying water sealing cover; (5) organic glass plate with holes; (6) filter cloth; (7) porewater storage tank; and (8) EKG.

The sediment used in the experiment was collected from an urban drainage channel, Fangcao Ditch (114°11′57.25″ E, 30°32′8.41″ N) in Wuhan, Hubei Province of China. The ditch primarily receives domestic wastewater from surrounding areas, characterized by black sediment with a foul odor and severe eutrophication. A total of 20 cm of surface sediment was collected and naturally dried after stones, branches, and other debris were removed. The sediment samples were then crushed and filtered through a 2-mm sieve. Experimental sediment with saturated moisture content was prepared using a blender and overlying water collected from the same sampling site. The fully mixed sediment was poured into an organic glass box (70 cm (L) × 60 cm (W) × 50 cm (H)) until the sediment reached a depth of 30 cm. a set of porewater drainage units was symmetrically inserted into the sediment with the upper edge positioned 2 cm below the sediment surface, maintaining a spacing of 30 cm between electrodes. (Figure 1c). To prevent the overlying water from directly penetrating into the EKG, the upper surface of the porewater drainage unit was placed 2 cm lower than sediment-water interface. Finally, deionized water was slowly siphoned along the edges of the box, forming a 20 cm overlying water layer. The experiment commenced after a clear and stable sediment-water interface was visually confirmed.

The indoor electrokinetic remediation experiments were performed at a constant room temperature of approximately 25 °C (Figure 1). According to the voltage gradients and drainage modes, the samples used in the experiments were divided into five groups: control (no voltage and no drainage), 0.0 V/cm (drainage under zero voltage plus gravity), 0.5 V/cm (intermittent power [IP] with 4 h on and 4 h off), 0.5 V/cm (continuous power

[CP] with 24 h on), and 1.0 V/cm (IP with 4 h on and 4 h off). A 30-V DC power supply (WYK-10020K, Sinole, Foshan, China) was used to provide constant voltage, and energy consumption was calculated according to the data recorded using an electric meter.

Throughout the experiment, cathode and anode effluents were collected. The volume of the effluent was recorded and used to determine the nutrient loads at different time intervals: daily in the first month and 3–10 days after the first month. Overlying water samples from ≥10 cm above the sediment-water interface were collected from the center of the experimental apparatus. The experiment lasted 88 days, and fresh sediment samples from top 5 cm layers below the sediment-water interface were collected near the anode and cathode by drilling through the side of the experimental apparatus (Figure 1). All the sediment samples were transferred into sterilized centrifuge tubes and stored at −20 °C for further nutrient and microorganism analysis. After aliquots were analyzed, the remaining electrode drainage was neutralized to pH 6–9 and, in accordance with the local sewer acceptance criteria, discharged to the sanitary sewer. This laboratory handling description does not constitute a field recommendation; field-scale effluent management is addressed in Section 4.5.

2.2. Sample Testing and Measurement

All the overlying water and electrode drainage samples were tested in duplicate. pH, electronic conductivity (EC), and dissolved oxygen (DO) concentrations of the samples were immediately measured using a pH meter (PB-10, Sartorius, Gottingen, Germany), conductivity meter (DDS-310, Leici, Shanghai, China), and portable DO meter (JPB-607A, Leici, Shanghai, China), respectively. TN and TP in overlying water column were determined using spectrophotometry after digestion with potassium persulfate, and the ammonia nitrogen (NH_4^+-N) and nitrate nitrogen (NO_3^--N) concentrations were measured through Nessler's reagent spectrophotometry and ultraviolet-visible spectrophotometry. Sediment pH and EC were measured using a pH and conductivity meter, with a water-to-sediment mass ratio of 1:5. Sediment organic matter (OM) content were determined using the loss on ignition (LOI) method at 550 °C for 4 h. The sediment moisture content was measured using a method that involved placing the sediment samples in an oven at 103–105 °C. Sediment TN and TP were measured using the potassium persulfate oxidation method and SMT method (Standards, Measurements, and Testing harmonized procedure for phosphorus fractionation in freshwater sediments), respectively [22].

Microbial DNA in the sediment was extracted in duplicate using a Power Soil DNA Isolation Kit (MoBio Laboratories, Carlsbad, CA, USA) according to the manufacturer's protocol. The V3-V4 region of the 16S rRNA gene was amplified using 12.5 ng of template DNA and the primers of 341F (F-5′-CCTACGGGNGGCWGCAG-3′) in a 30-μL PCR reaction. The concentration and purity of the extracted DNA were assessed using a Nanodrop Spectrophotometer ND-2000 (Thermo Fisher Scientific, Waltham, MA, USA). Sequencing libraries were then constructed using a TruSeq Nano DNA LT Library Prep Kit (Illumina, Inc., San Diego, CA, USA) according to the manufacturer's instructions and associated index codes. The library was sequenced on an Illumina NovaSeq 6000 platform (Illumina, Inc., San Diego, CA, USA) at Wuhan Benagen Technology (Wuhan, China). Cutadapt software (v.3.5) was used to identify and remove primer sequences and to perform length filtering to obtain clean sequences. To identify feature sequences (amplicon sequence variants, ASVs), DADA2 was used to process raw data, merge paired-end reads, and remove chimeric sequences. Subsequently, QIIME2 software (https://qiime2.org/ (accessed on 14 May 2024)) was applied to filter out low-abundance ASVs. Finally, bacterial ASVs were assigned to taxonomic groups using the SILVA database (https://www.arb-silva.de/ (accessed on 14 May 2024), and alpha diversity indices-including the Shannon, Simpson, and Chao1 indices, as well as the abundance-based coverage estimator (ACE)-were calculated using QIIME2 software.

2.3. Data Processing and Analysis

All statistical analyses were performed using SPSS 23.0 software. Pearson's correlation coefficients were calculated to examine relationships between the parameters of interest. One-way analysis of variance (ANOVA), followed by Tukey's test ($p \leq 0.05$), was used to evaluate differences in nutrient drainage among the experimental groups. The genera with 10 highest relative abundances were selected for inclusion in a redundancy analysis (RDA), which quantitatively assessed the effects of certain factors, including sediment pH value and moisture content, on microbial communities. Figures were generated using Origin 2018 software.

The water balance in each experimental apparatus was calculated as follows:

$$\Delta S + \Delta H = \Sigma D + \Sigma V + \Sigma S + \Delta \quad (1)$$

where ΔS is the change in sediment porewater volume, calculated from the difference in sediment moisture content before and after treatment; ΔH is the change in overlying water volume in the organic glass box, determined by

the change in water level; Σ*D*, Σ*V*, and Σ*S* represent the total volumes of anode and cathode effluent, evaporated overlying water, and collected samples, respectively; and Δ is the measurement error.

Nutrient removal due to electrode drainage was calculated as follows:

$$Q = \sum_{i=1}^{n} C_i V_{\mathrm{w}i} \tag{2}$$

where Q is the total amount of nutrient removed (mg); n is the number of samples; C_i is the nutrient concentration in the ith sample of electrode drainage (mg/L); $V_{\mathrm{w}i}$ is the volume of the ith electrode drainage sample (L). The nutrient release flux at the sediment-water interface was calculated using the following equations [19]:

$$R = V_n C_n + \sum_{i=1}^{n} V_{si} C_{si} - V_0 C_0 \tag{3}$$

$$F_{\mathrm{t}} = \frac{R}{S\Delta \mathrm{t}} \tag{4}$$

where R is the cumulative amount of nutrients released from sediment (mg), with positive R values indicating nutrient release (source) and negative R values indicating nutrient absorption (sink); C_{si} is the average nutrient concentration of the ith overlying water samples (mg/L); V_{si} is the volume of the ith overlying water sample (L); C_0 and $C_n$are the initial and final nutrient concentrations of the overlying water (mg/L); V_0 and C_n are the initial and final volume of the overlying water samples (L); F_{t} is nutrient release flux during the time interval between $t_{\mathrm{n-1}}$ and t_{n} [mg/(m^2·d)]; S is the total surface area of the SWI (m^2); and Δt is the time interval $t_{\mathrm{n}}-t_{\mathrm{n-1}}$ (d). Nutrient loss through evaporation was not considered in Equations (3) and (4).

The power consumption E (kW·h·g^{-1}) was calculated using the following equation [5]:

$$E = \frac{1}{1000m} \int_0^t UIdt \tag{5}$$

where m is the wet weight of the treated sediment t, U is the applied voltage between the electrodes (V), I is the electric current (A), and t is the duration of treatment (h).

3. Results

3.1. Variation in Nutrients Content of Overlying Water

Throughout the experiment, average pH of the overlying water ranged from 8.05 to 8.17, and no significant difference was observed between the experimental and control groups. DO concentrations in all the treatment groups generally decreased from 5.96–7.26 to 3.41–5.69 mg/L with slight fluctuations (Figure S1). EC increased continuously over time, and significant differences were identified among different groups. Control group had the highest EC, followed by the 0 V/cm group (Table 1, Figure S1).

The average concentrations of TN in the overlying water samples ranged from 2.27 to 4.37 mg/L (Table 1). It was significantly higher in the control group than in the experimental groups ($p < 0.05$). NH_4^+-N comprised most of the TN. Porewater drainage greatly reduced the NH_4^+-N/TN concentrations in the overlying water. For example, in 0.0 and 1.0 V/cm groups, the NH_4^+-N/TN concentrations initially ranged from 28.68–75.05% but markedly decreased to 13.09–46.49% after 12–16 days of treatment (Figure S2). The NH_4^+-N/TN concentrations tended to stabilize after 46 days, and the final NH_4^+-N/TN concentrations in the control, 0.0 V/cm, and 1.0 V/cm group were 55.27%, 12.96%, and 8.69%, respectively (Figure S2).

TP concentration in the overlying water was initially low (0.03 mg/L) and fluctuated throughout the treatment. Compared with the control group, the final TP concentrations in the overlying water samples in the experimental groups (0.054, 0.043, 0.049, and 0.075 mg/L in the 0.0 V/cm, 1.0 V/cm, 0.5 V/cm [IP], and 0.5 V/cm [CP] groups, respectively) were 34–105% higher than that in the control group. Porewater drainage through EKG affected phosphorus concentrations in the overlying water (Figure S2). The SRP/TP ratio in the control group generally increased over time, whereas the SRP/TP ratios in the 0.0 and 1.0 V/cm groups gradually decreased after peaking at 59.61–95.79% after 34–46 days of drainage (Figure S2).

The porewater drainage also affected the TN/TP mass ratio in the overlying water. The TN/TP ratio in the control group gradually increased from 89.2 to 315.9 during the experiment, whereas in the 0.0 and 1.0 V/cm groups it decreased after a weak increase within the range of 27.3–144.5 (Figure S2).

Table 1. Mean values ± standard deviations of water quality parameters of overlying water and electrode drainage (n = 30).

Sample		Parameters	0.0 V/cm NP	1.0 V/cm IP	0.5 V/cm IP	0.5 V/cm CP	Control
Overlying water		pH (-)	8.05 ± 0.32	8.09 ± 0.35	8.17 ± 0.28	8.10 ± 0.34	8.06 ± 0.24
		EC (μS/cm)	641 ± 161 ^{a,b}	591 ± 211 ^{b,c}	487 ± 146 ^{c,d}	455 ± 130 ^{d}	740 ± 185 ^{a}
		DO (mg/L)	5.56 ± 1.00	5.32 ± 1.00	5.39 ± 1.04	5.54 ± 1.16	5.79 ± 0.61
		TP (mg/L)	0.046 ± 0.009 ^{a}	0.045 ± 0.011 ^{a}	0.044 ± 0.010 ^{a}	0.046 ± 0.014 ^{a}	0.033 ± 0.006 ^{b}
		SRP (mg/L)	0.015 ± 0.011	0.017 ± 0.014	0.018 ± 0.013	0.018 ± 0.016	0.011 ± 0.009
		TN (mg/L)	2.92 ± 0.79 ^{b}	2.75 ± 1.04 ^{b}	2.32 ± 0.77 ^{b}	2.27 ± 0.75 ^{b}	4.37 ± 1.84 ^{a}
		NH_4^+-N (mg/L)	2.11 ± 0.97	2.17 ± 1.13	1.73 ± 0.73	1.81 ± 0.68	2.02 ± 1.10
		NO_3^--N (mg/L)	0.68 ± 0.35 ^{b}	0.54 ± 0.24 ^{b}	0.55 ± 0.21 ^{b}	0.43 ± 0.15 ^{b}	2.28 ± 0.92 ^{a}
Drained effluent	Anode	pH (-)	7.12 ± 0.24 ^{a}	2.98 ± 1.75 ^{c}	5.59 ± 1.98 ^{b}	4.83 ± 1.83 ^{b}	/
	Cathode		7.17 ± 0.27 ^{c}	12.32 ± 1.14 ^{a}	9.34 ± 2.49 ^{b}	10.52 ± 2.10 ^{b}	
	Anode	EC (μS/cm)	4955 ± 423 ^{b}	7721 ± 3176 ^{a}	5015 ± 1221 ^{b}	4979 ± 3106 ^{b}	/
	Cathode		4707 ± 472 ^{b}	6495 ± 2969 ^{a}	4703 ± 1866 ^{b}	4349 ± 3175 ^{b}	
	Anode	TP (mg/L)	1.93 ± 1.63 ^{b}	5.71 ± 3.96 ^{a}	1.05 ± 0.77 ^{b}	1.26 ± 1.54 ^{b}	/
	Cathode		2.47 ± 2.20 ^{a}	0.53 ± 0.14 ^{b}	0.74 ± 0.21 ^{b}	0.76 ± 0.35 ^{b}	
	Anode	SRP (mg/L)	0.70 ± 0.55 ^{b}	5.27 ± 3.81 ^{a}	0.70 ± 0.80 ^{b}	0.98 ± 1.56 ^{b}	/
	Cathode		0.99 ± 0.91 ^{a}	0.32 ± 0.12 ^{b}	0.32 ± 0.12 ^{b}	0.32 ± 0.13 ^{b}	
	Anode	TN (mg/L)	26.29 ± 5.59 ^{a}	18.19 ± 3.36 ^{c}	22.27 ± 5.64 ^{b}	17.28 ± 3.44 ^{c}	/
	Cathode		22.61 ± 4.78 ^{b}	51.08 ± 19.24 ^{a}	45.79 ± 14.79 ^{a}	47.01 ± 12.59 ^{a}	
	Anode	NH_4^+-N (mg/L)	19.69 ± 3.90 ^{a}	12.56 ± 3.62 ^{c}	17.00 ± 3.17 ^{b}	13.35 ± 2.34 ^{c}	/
	Cathode		18.05 ± 4.21 ^{b}	47.41 ± 16.64 ^{a}	45.65 ± 13.45 ^{a}	39.33 ± 13.27 ^{a}	

Means marked with different letters differ significantly different from each other at $p \leq 0.05$ (Tukey's test); NP, IP, and CP stand for *not powered*, *intermittently powered*, and *continuously powered*, respectively, and n is the sampling number; the same below.

3.2. Trends in Nutrient Release Flux

Porewater drainage significantly restrained nitrogen release. Throughout the experiment, TN release flux at the SWI in the control group ranged from 33.68 to 188.15 mg/(m^2·d), whereas those in the experimental groups ranged from −15.70 to 79.90 mg/(m^2·d) (Figure 2). Among the experimental groups, 0.0 and 1.0 V/cm groups showed the highest and lowest TN release fluxes, respectively. Compared with the control group, TN release flux under gravity porewater drainage (0.0 V/cm) decreased by 76.72%. In the 1.0 V/cm group, the TN release flux was reduced by over 95.53% compared with the control group. Moreover, nitrogen release at the SWI primarily occurred during the first month of the experiment (Figure 2), after which the net release flux gradually declined to zero due to continuous porewater drainage.

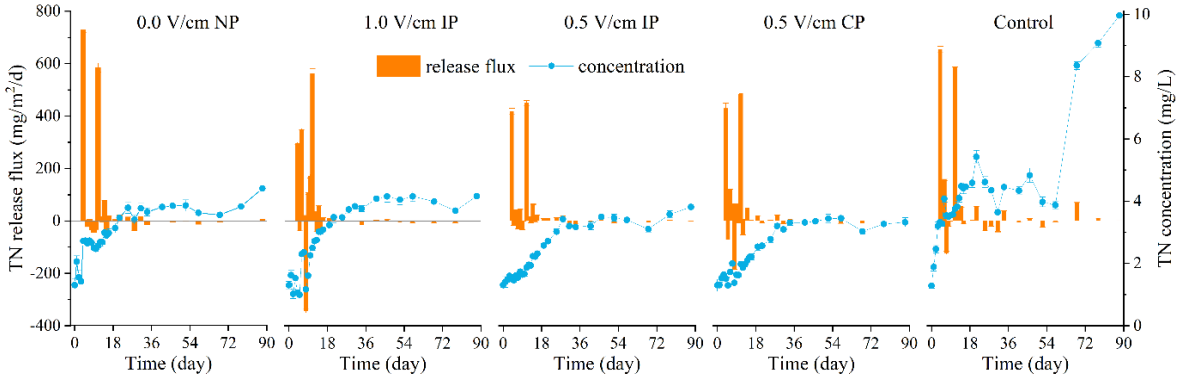

Figure 2. Variations in TN concentrations in overlying water and TN release flux from sediment.

Throughout the experimental period, the TP release flux at the SWI fluctuated between −3.56 and 4.28 mg/(m^2·d). During the initial stage (0–28 days), the TP release flux at the SWI showed significant fluctuations, alternating between release and absorption. Subsequently, after nearly 70 days of treatment, the TP release flux in all the groups except the control group decreased to negative values (Figure 3). This suggests that an increasing amount of phosphorus from the overlying water was absorbed into the sediment, shifting the sediment from a phosphorus source to a sink due to continuous porewater drainage.

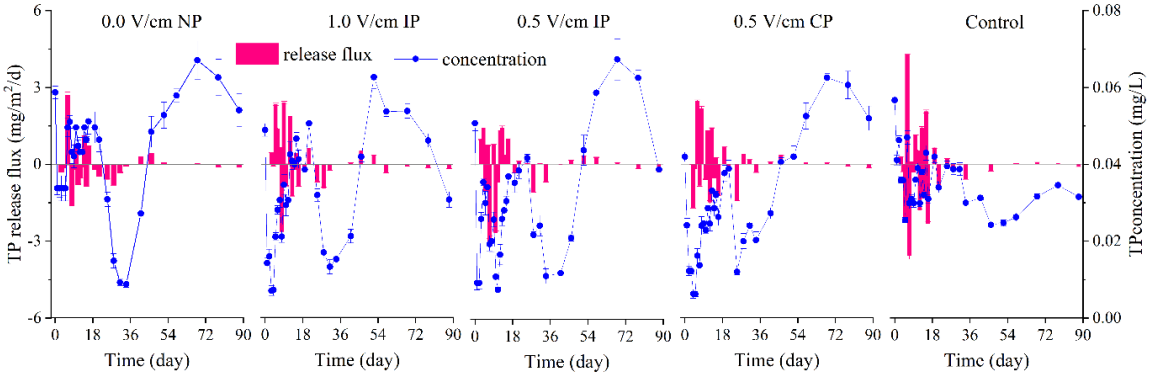

Figure 3. Variations in TP concentrations in overlying water and TP release flux from sediment.

3.3. Nutrients Content of Electrode Drainage Water

In the absence of an electric field, the average pH and EC of the electrode drainage ranged from 7.12 to 7.17 and 4707 to 4955 μS/cm, respectively. The physicochemical properties of drainage samples under electric field conditions differed significantly from those of the control group. Anode drainage was acidic, with average pH ranging from 2.98 to 5.59 and EC ranging from 4979 to 7721 μS/cm. Cathode drainage was alkaline, with average pH ranging from 9.34 to 12.32 and EC ranging from 4349 to 6495 μS/cm (Table 1). Voltage gradients strongly affected the drainage pH and EC. Stronger voltage gradients resulted in greater variations in drainage pH and EC. In contrast, variations in drainage pH and EC were more moderate in the IP groups (Table 1).

In the absence of electric field, differences between the anode and cathode drainage were negligible, with average TP and TN concentrations ranging from 1.93 to 2.47 mg/L and 22.61 to 26.29 mg/L, respectively. Nutrient

concentrations in electrode drainage were significantly higher than in the overlying water (Table S1). Under electric field conditions, TP and TN were primarily drained from the anode and cathode, respectively. TP and TN concentrations ranged from 1.0 to 5.71 and from 45.79 to 51.08 mg/L, respectively (Table 1). In both the cathode and anode effluents, SRP and NH_4^+-N accounted for the largest proportions of phosphorus (41.64–79.75%) and nitrogen (80.33–93.70%), respectively (Table 1).

During the experiment, cumulative porewater drainage volume ranged from 30.3–51.0 L (Table 2). Porewater was mainly drained from the cathode, with the average volume of cathode drainage approximately 1.01–1.63 times higher than that of anode drainage. The stronger the voltage gradient was, the greater volume of the drainage. The cumulative volumes of cathode drainage in the 1.0 V/cm (IP) and 0.5 V/cm (IP) groups were 26.8 and 17.7 L, respectively. Under the same voltage gradient, nutrient separation performance in the CP groups was notably greater than in the IP groups. During the experiment, the cumulative amounts of discharged TN in the 0.0 V/cm, 1.0 V/cm, 0.5 V/cm (IP), and 0.5 V/cm (CP) groups were 718.11, 1711.33, 1284.96, and 1308.11 mg, respectively, while the cumulative amounts of discharged TP were 88.44, 107.06, 35.20, and 42.56 mg, respectively.

Table 2. Water balance calculations for different experimental groups.

Treatment Groups	Anode Drainage (L)	Cathode Drainage (L)	ΔS (L)	Σ (L)	ΔH (L)	Σ/ΔH (%)
0.0 V/cm NP	15.10	15.20	2.70	30.30	35.70	84.87
1.0 V/cm IP	16.48	26.81	2.70	45.98	51.00	90.17
0.5 V/cm IP	17.00	17.72	2.70	37.42	39.45	94.84
0.5 V/cm CP	17.06	19.24	2.70	41.00	47.55	86.23

NP, IP, and CP stand for not powered, intermittently powered, and continuously powered, respectively.

3.4. Changes in Sediment Nutrients and Microbial Community

Porewater drainage through EKG affects various physicochemical parameters of sediment. Porewater drainage exerted a non-significant influence on the sediment pH. The average sediment pH in the anode and cathode zones ranged from 7.29 to 7.63 and 7.45 to 7.79, respectively (Table 3). However, the sediment EC varied from the anode zone to the cathode zone within the range of 727–1137 μS/cm, and the maximum and minimum EC occurred in the cathode zone in the 1.0 V/cm (IP) group and in the anode zone in the 0.5 V/cm (CP) group, respectively. Porewater drainage resulted in a decline in the sediment moisture content. The average sediment moisture content ranged from 36.54% to 39.12% in the experimental groups, compared with 39.69% in the control group. Due to nutrient removal by porewater drainage, sediment TN and TP contents decreased, particularly TP in the anode zones and TN in the cathode zones (Table 3). The experimental groups exhibited 1.06–5.02% and 2.65–13.63% decreases in sediment TP and TN contents, respectively, compared with the control group after 88 days of treatment.

Table 3. Major physiochemical parameters of different treatment sediments.

Parameters		After Different Treatment				
		0.0 V/cm NP	1.0 V/cm IP	0.5 V/cm IP	0.5V/cm CP	Control
Anode zone	pH	7.52 ± 0.03	7.29 ± 0.06	7.41 ± 0.03	7.63 ± 0.18	7.74 ± 0.23
Cathode zone		7.50 ± 0.04	7.45 ± 0.06	7.53 ± 0.06	7.79 ± 0.08	
Anode zone	EC (μS/cm)	881 ± 11	1137 ± 51	901 ±4 9	727 ± 93	729 ± 21
Cathode zone		951 ± 101	1012 ± 15	836 ± 39	775 ± 115	
Anode zone	LOI (%)	9.05 ± 0.07	8.93 ± 0.35	9.02 ± 0.74	8.43 ± 0.24	9.43 ± 0.25
Cathode zone		9.17 ± 0.03	9.38 ± 0.53	7.93 ± 0.19	8.48 ± 0.12	
Anode zone	Moisture content	38.37 ± 1.24	38.87 ± 2.71	37.92 ± 2.30	37.61 ± 1.56	39.69 ± 0.92
Cathode zone	(%)	36.54 ± 1.34	37.80 ± 0.84	39.12 ± 1.41	37.86 ± 1.44	
Anode zone	TP (mg/kg)	1483 ± 44	1497 ± 33	1489 ± 7	1487 ± 20	1513 ± 36
Cathode zone		1442 ± 29	1437 ± 63	1482 ± 27	1441 ± 28	
Anode zone	TN (mg/kg)	1250 ± 56	1097 ± 77	1109 ± 60	1192 ± 46	1284 ± 78
Cathode zone		1261 ± 42	1281 ± 25	1144 ± 13	1145 ± 49	

Mean values represent the averages of bilateral electrode sampling sites; the same below.

The effects of porewater drainage on the microbial communities in the sediments were negligible. The different experimental groups shared the same dominant species of microorganism (Figure S3). The phyla with the highest relative abundances in the microbial community were *Proteobacteria* (19.77%), *Bacteroidetes*

(19.46%), *Chloroflexi* (12.85%), *Acidobacteria* (9.59%), *Actinobacteria* (7.60%), *Myxococcota* (7.31%), *Patescibacteria* (7.05%), *Firmicutes* (4.62%), *Gemmatimonadota* (2.58%), and *Planctomycetota* (2.31%). The effects of porewater drainage on the microbial community structure and abundance in the sediment were also nonsignificant. Compared with the control group, the experimental groups had slightly higher Shannon and Simpson indices values and non-significantly lower Chao1 and ACE indices (Table 4). Voltage gradients were strongly negatively correlated with the microbial community species abundance. The 1.0 V/cm IP group had the lowest Chao1 and ACE indices (2127.25 and 2123.12, respectively).

Table 4. Alpha diversity indices of microbial communities in sediments after different treatments.

Group	Shannon	Simpson	Chao1	ACE
0.0 V/cm NP	9.536 ± 0.042	0.996 ± 0.001	2287.426 ± 53.23	2263.38 ± 62.87
1.0 V/cm IP	9.480 ± 0.118	0.996 ± 0.001	2127.25 ± 184.92	2123.12 ± 179.62
0.5 V/cm IP	9.416 ± 0.204	0.995 ± 0.002	2242.51 ± 42.47	2234.39 ± 38.48
0.5 V/cm CP	9.428 ± 0.081	0.995 ± 0.001	2150.88 ± 89.23	2145.58 ± 86.93
Control	9.278 ± 0.106	0.992 ± 0.002	2265.70 ± 40.13	2270.95 ± 38.78

4. Discussion

4.1. Differences between N and P Release due to Porewater Drainage

Porewater drainage exerted distinct effects on the release of nitrogen and phosphorus. Sediment TN release flux sharply decreased to ≤10% of its maximum value within 14 days of drainage, whereas TP release flux continually fluctuated (Figures 2 and 3). The TP release flux began to exhibit a clearly downward trend only after nearly 28 days of drainage. For both nitrogen and phosphorus, the drainage of porewater changes the role of sediment from source to sink and effectively restrained nutrients increase in overlying water.

The nitrogen and phosphorus drainage also responded differently to voltage gradients. The presence of electric field greatly enhanced the nitrogen drainage, and cathode effluent NH_4^+-N concentrations in the 0.5 and 1.0 V/cm groups were 2.2–2.4 times higher than that in 0.0 V/cm group (Figure S4). However, the TN drainage concentrations in the 0.5 and 1.0 V/cm groups did not differ significantly (Table 1). Regarding phosphorus drainage, the anode effluent SRP concentration in the 0.5 V/cm group was not significantly higher than that in the 0.0 V/cm group. As voltage gradient increased from 0.5 V/cm to 1.0 V/cm, the anode effluent TP concentrations rapidly increased from 0.37 mg/L to a peak of 12.68 mg/L within 14 days (Figure S4), whereas cathode effluent TP concentrations remained low.

Because of the difference between nitrogen and phosphorus drainage processes, the TN/TP ratio in the overlying water changed greatly over time. It continually increased in the control group but tended to decrease after a slight initial increase in the experimental groups (Figure S2). Overall, porewater drainage significantly reduced the TN/TP ratios in the overlying water of all groups.

Throughout the experiment, the cumulative energy consumption ranged between 0.71–3.93 kW·h, and the calculated energy consumption intensity for nitrogen and phosphorus separation through porewater drainage ranged between 0.55–2.30 kW·h/g and between 20.04–36.76 kW·h/g, respectively. The energy consumption in the IP groups was 32.8% lower than in the CP groups. Considering both of the energy consumption and nutrient separation efficiency, IP mode probably is more economical. The most suitable voltage gradients for restricting sediment phosphorus and nitrogen release were 1.0 and 0.5 V/cm, respectively. The overall cost of EKG is typically governed by reagent consumption and resource-recovery credits rather than electricity alone. The electricity figures reported here serve process characterization; a full techno-economic analysis (TEA) will be provided separately with scale-up and field validation.

4.2. Physical Processes Regulating Sediment Nutrient Release

In the presence of overlying water, porewater drainage compressed the pores in surface sediment layers, thereby directly reducing the potential for nutrient release. According to Fick's diffusion law, static sediment nutrient release flux mainly depends on the concentration gradient of nutrients and sediment porosity [23]. In the present study, because of porewater drainage, the average sediment thickness was decreased by 0.3–0.8 cm, and the total sediment volume was decreased by about 2 L. The SWI collapsed, and the surface sediment porosity was decreased by nearly 30% (Figure 4). Compression of sediment pores inhibited the release of porewater into the overlying water, thereby restricting nitrogen and phosphorus release from surface sediment.

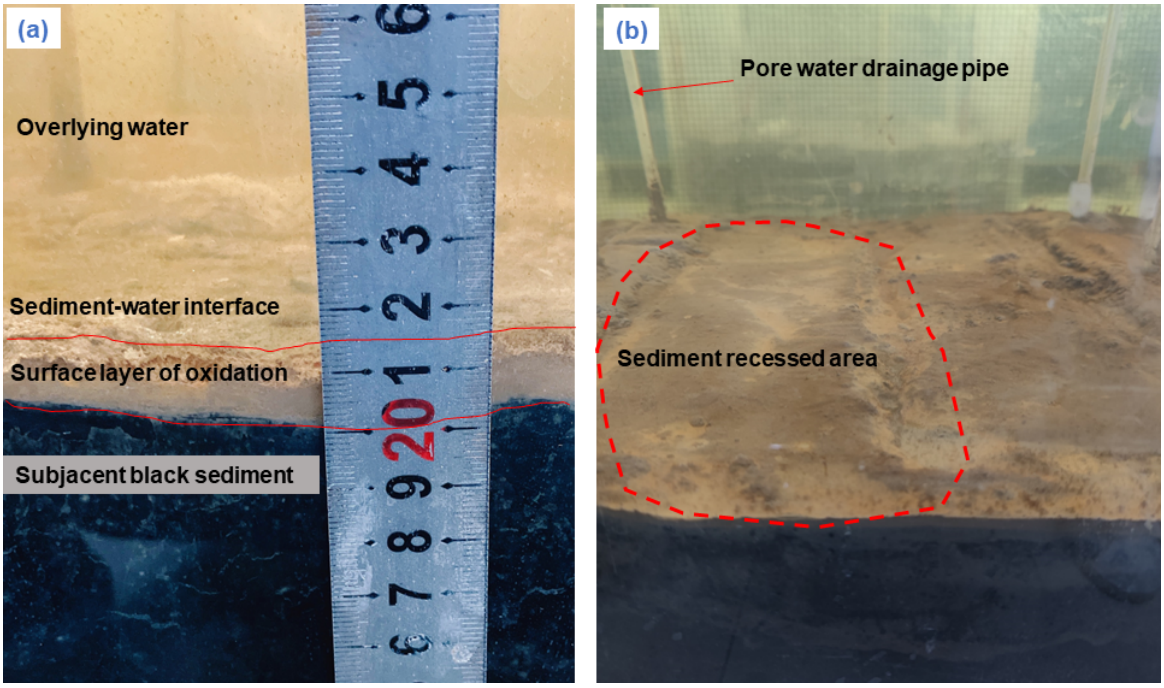

Figure 4. Changes in sediment appearance due to pore water drainage via EKG: (**a**) profile color and (**b**) surface morphology.

The recharge and renewal of porewater further reduced the capacity of surface sediment releasing nutrients. Water balance calculations (accounting for water losses due to sampling and evaporation, Table 2) indicated that 29.4–49.2 L of overlying water entered the sediment during the experiment, replenishing 49–82% of porewater. Nitrogen and phosphorus concentrations in the overlying water were significantly lower than those in porewater, and drained porewater TN and TP concentrations were 11.1–123.3 and 7.22–22.7 times higher, respectively (Table 1). The infiltration of overlying water into surface sediment pores effectively diluted porewater nutrient concentrations and reduced their potential release. Furthermore, the combined effects of overlying water infiltration, porewater drainage, and nutrient removal created a dialysis-like effect, facilitating nutrient content reduction in the overlying water, porewater, and sediment particles.

4.3. Chemical Processes Influencing Sediment Nutrient Release

Improved oxidation conditions can inhibit sediment nutrient release. Under natural conditions, DO typically penetrates sediments to depths of less than 1 cm [9]. Degradation of OM usually lowers sediment redox potential and produces anaerobic environments [24], thereby promoting the reduction of Fe (III) and associated liberation of phosphorus bound to Fe (III) [6]. In contrast to anaerobic conditions, aerobic conditions favor the formation of Fe(III)-phosphate complexes, inhibiting soluble phosphate release from sediment to overlying water [25]. Aerobic conditions restrict the release of ammonia nitrogen into overlying water. The release flux of NH_4^+-N under aerobic conditions is much lower than under anoxic conditions [26]. In this study, porewater drainage through EKG strengthened the sediment oxidation conditions. First, DO penetrated the surface sediment layer, and the porewater was replenished with overlying water. This oxygenated the SWI and restricted the release of nitrogen and phosphorus. Second, the electrolysis of porewater in the anode zone produced oxidizing substances such as oxygen, hydroxyl radicals, and active chloride ions [12], which created aerobic environments for the surface sediment. Ammonia nitrogen in the anode zone can be directly oxidized to evaporable N_2 [27,28]. During the experiment, the color of the SWI gradually changed from black to gray and yellow, extending into deeper sediment layers over time (Figure 4), indicating that DO and oxidizing substances had penetrated into the deeper sediment layers and restricted the release of nitrogen and phosphorus.

Porewater drainage through EKG influenced nutrient transfer and transformation. Electromigration promotes the accumulation of sediment phosphate and ammonia nitrogen in the anode and cathode zones, respectively. Electrolysis of porewater in the anode zone resulted in sediment acidification due to the accumulation of H^+, which promoted the activation of carbonate-bound phosphorus and iron–manganese oxide-bound phosphorus [20]. By inducing changes in pH, variations in sediment iron species and OM affected phosphorus transformation. Under acidic conditions (pH < 4.0), Fe (III) existed in ionic form, and phosphorus bound to Fe (III) was released into

porewater and drained through anode effluent. In contrast, under alkaline conditions, Fe (III) was precipitated into minerals, which reduced the mobility of phosphorus [29,30]. In our former study, porewater drainage through EKG caused a 41.02% decrease in sediment amorphous iron oxide content, which promoted iron-bound phosphorus removal [20]. In addition, Ca^{2+}, Mg^{2+}, and other metal ions migrated and accumulated in the alkaline cathode zone. A small amount of phosphorus was therefore retained in granular form as it crystallized and coprecipitated with the metal ions [20].

Ammonia nitrogen was a major component of porewater TN, and electromigration and volatilization were the main mechanisms underlying ammonia nitrogen removal during electrokinetic porewater drainage. Because NH_4^+-N was positively charged, most of the TN migrated to and accumulated in the cathode zone. The NH_4^+-N concentrations in the cathode drainage gradually increased and remained at about 77.82 mg/L, but the NH_4^+-N concentrations in the effluents only slightly increased in the absence of electric field (Figure S4). Ammonia nitrogen in water columns mainly existed in the form of molecular NH_3 and ionic NH_4^+; NH_3 concentrations are primarily dependent on pH and temperature [31,32]. Previous study found that the proportion of NH_3 was higher than that of NH_4^+ when the pH value exceeded 9.25 [33]. In our work, in the presence of an electric field, positively charged ammonia nitrogen migrated to the cathode zone. Substantial OH^- generated through porewater electrolysis also accumulated in the cathode zone, resulting in an alkaline effluent with a pH of 9.10–13.36 (Figure S5). This explains why, in the presence of an electric field, some NH_3 in the alkaline cathode zone directly escaped as gas because of the Joule heating effect produced by the EKG [34], and some NH_3 was converted into N_2 and NOx through electrochemical reactions [35].

4.4. Microbial Responses to Porewater Nutrient Drainage

Physicochemical processes, including sediment pore compression, porewater renewal and drainage, electromigration, and electrochemical oxidation, regulated sediment nutrient release. A comparison between the powered groups and non-powered group revealed that porewater gravity drainage was responsible for 42.0% and 83.3% of the total separation of TN and TP, respectively (Table 2). This suggested that the physical processes involved in porewater drainage were the main mechanism underlying the reductions in the release flux of sediment nutrients. Under natural conditions, the release of nutrients from surface sediment can last decades or even centuries [36]. When the electric field was applied, most of the SRP and NH_4^+-N were drained within the first month. Increases in the voltage gradient accelerated this process and increased the ratios of SRP/TP and NH_4^+-N/TN (Figure 5). Therefore, porewater drainage through EKG can rapidly reduce the content and release flux of sediment nutrients, thus shortening the duration of eutrophic water remediation.

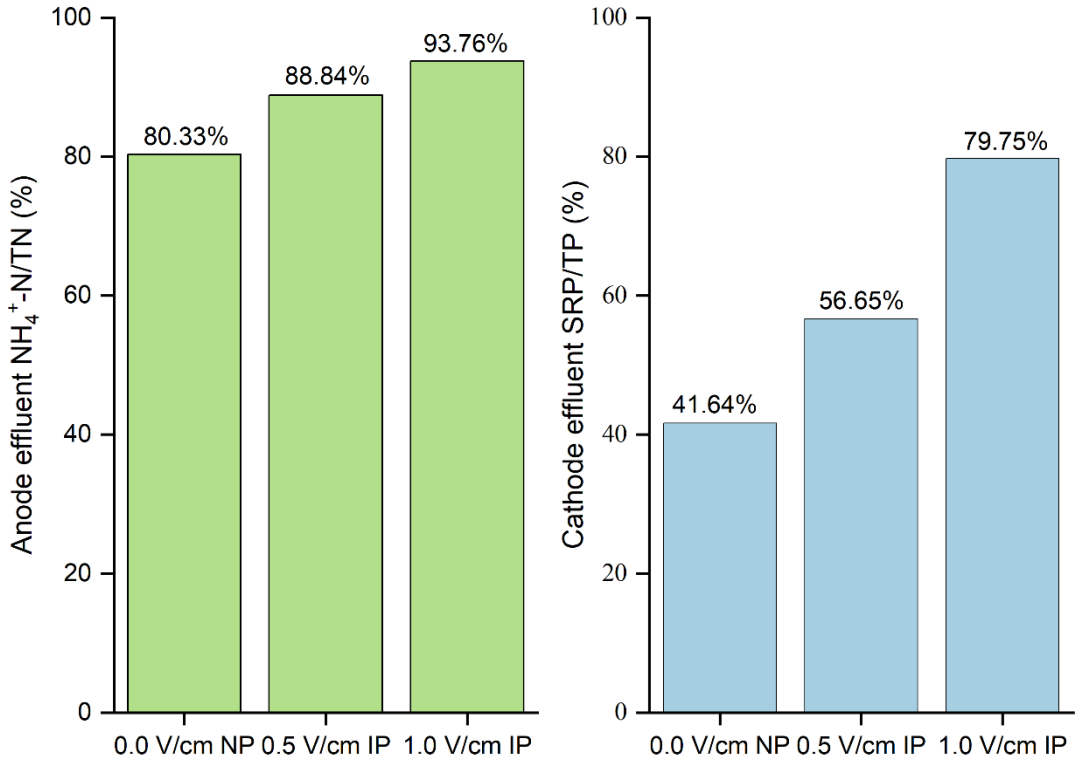

Figure 5. Average effluent NH_4^+-N/TN and SRP/TP ratios of representative experimental groups.

At the experiment's end, the control exhibited a significantly lower Shannon index than the electrokinetic treatments (Table 4), implying that electro-drainage tempered dominance by a few taxa and modestly broadened diversity. Directional porewater advection likely disrupted spatially clustered populations and facilitated their lateral spread within the sediment [37]. In parallel, downward transport of overlying water during electrokinetic dialysis may have episodically supplied aerobic lineages, increasing niche heterogeneity [38]. By diminishing selective pressures associated with elevated ammonium or extreme pH, drainage could also narrow the competitive advantage of highly tolerant specialists and allow less abundant taxa to persist [39].

Prior reports show that moderate electrothermal effects (e.g., 2 V/cm) can even stimulate microbial activity [40,41], suggesting the electric field itself is unlikely to broadly impair viability. The occasional decline in richness is more plausibly linked to localized pH excursions-alkalinization at the cathode and acidification at the anode-that exceed tolerance windows for subsets of the community [39,42]. Consistently, our RDA identified pH as the dominant explanatory variable, whereas EC, WC, TP, and TN contributed far less (Figure 6). Mechanistically, pH stress can perturb membrane integrity and electrochemical gradients, rewire metabolic pathways, and selectively suppress acid-tolerant taxa near cathodes and alkali-tolerant taxa near anodes [43]. As one example, members of Bacteroidetes exhibit narrow pH optima-growth peaks around pH 6.7, declines near 6.0, and is strongly inhibited at 5.5 [44]. Additionally, incomplete replenishment of porewater after drainage could transiently deplete bioavailable N and P, compounding growth limitations [45].

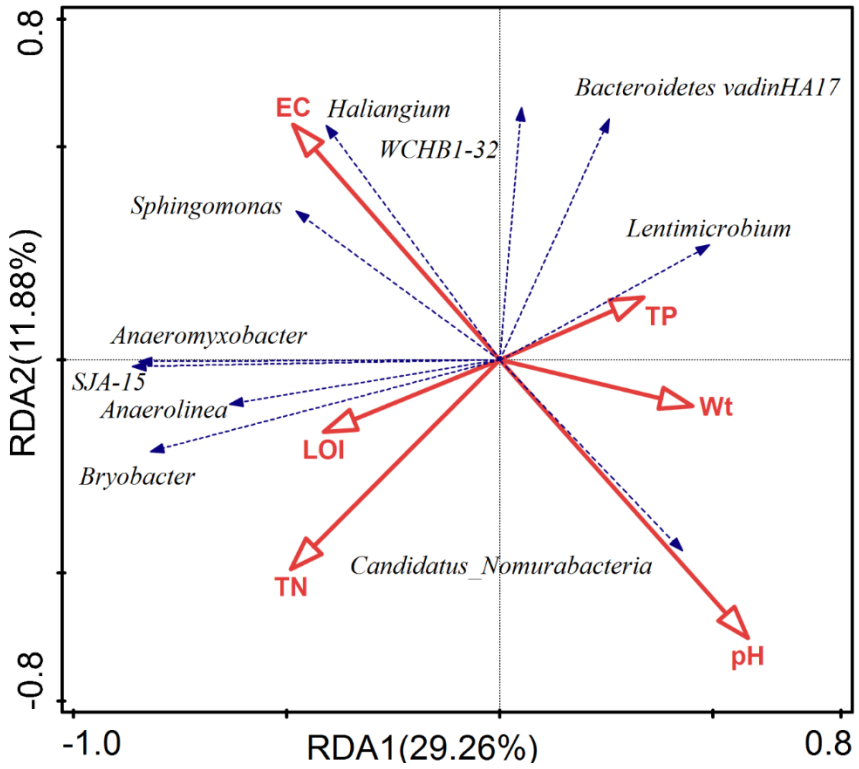

Figure 6. RDA of microbial communities in and physiochemical parameters of sediment. Blue arrows indicate species in the 10 most abundant genera, and red arrows indicate physiochemical parameters of sediment. The relationship between the microbial species and sediment parameters is reflected in the included angles; obtuse and acute angles represent negative and positive correlations, respectively.

The ACE and Chao l index reflect the abundance of microbial species. The ACE and Chao l indices of the 1.0 V/cm group were non-significantly lower than those of the control group (6.11% and 6.51% lower respectively, Table 4). Moreover, the Simpson and Shannon indices did not differ significantly among the groups, indicating that the influence of porewater drainage through EKG on the sediment microbial community was negligible. Previous study has found that weak DC electric fields (<2.0 V/cm) exert non-significant negative effect on the viability of microorganisms [40]. In addition, Li et al. [41] reported that the thermal effect generated by a 2-V/cm electric field is beneficial to the growth and metabolism of microorganisms. Therefore, in the present study, porewater drainage in an electric field with a voltage gradient of ≤1.0 V/cm could not negatively affect the sediment ecosystem.

We did not assay functional genes, so a microbial contribution cannot be fully excluded. However, the charge-selective partitioning of NH_4^+ (to the catholyte) and SRP (to the anolyte), together with the strongly acidic/alkaline electrode effluents, is more consistent with electromigration and pH-driven speciation/precipitation, and the broadly stable community structure supports this view. Future work will pair functional-gene/qPCR or metagenomics with isotope/tracer tests to quantify biotic versus abiotic contributions.

4.5. Implications for Application

Electrokinetic dialysis technology, using EKGs to drain sediment porewater, enables the rapid migration and separation of nutrients under in-situ conditions. Compared with traditional sediment remediation techniques, electrokinetic dialysis avoids extensive sediment excavation and transportation, thereby significantly reducing the high costs and secondary pollution risks associated with environmental dredging. Unlike capping techniques, which only block nutrient release but cannot effectively remove nutrients, electrokinetic dialysis fundamentally reduces the potential for internal nutrient loading. Additionally, porewater drainage quickly reduces sediment porosity and enhances sediment oxidation conditions, markedly shortening the duration of ecological restoration for eutrophic waterbodies and demonstrating strong potential for field application. Importantly, this study revealed that EKG-driven porewater drainage did not negatively affect sediment microbial abundance or community structure, highlighting the ecological friendliness and sustainability of electrokinetic remediation in preserving sediment ecological stability.

However, several challenges remain to be addressed. The drained porewater typically exhibits high nutrient concentrations and contains various metal cations and anions, necessitating effective downstream wastewater treatment to prevent secondary pollution. Electrokinetic drainage produces two small-volume sidestreams: an alkaline, NH_4^+-N-rich catholyte and an acidic, soluble reactive phosphorus-rich anolyte. A practical approach is controlled co-neutralization to reduce downstream reagent demand, followed by nutrient recovery-prioritizing struvite crystallization when the P/N ratio is favorable, and, where phosphorus is limiting, treating the catholyte by air stripping with acid scrubbing or by ion exchange. Furthermore, laboratory-scale findings require validation in terms of effectiveness and economic feasibility under real-world conditions, especially concerning large-scale or complex natural environments, long-term equipment stability, and energy consumption. Future research should focus on field-scale pilot or demonstration projects to assess the long-term performance and economic viability of electrokinetic dialysis, optimize operational parameters, and thus facilitate its broader application in sediment remediation of eutrophic waterbodies.

Electrode drainage from the EKG device is low-volume but high-strength: anode streams are typically acidic and SRP-rich, whereas cathode streams are alkaline and NH_4^+-rich. At laboratory scale, after aliquots were analyzed, the remaining drainage was neutralized to pH 6–9 and discharged to the sanitary sewer. For field deployment, we recommended a concise pre-treatment train to ensure compliance and minimize scaling: segregated collection of anode/cathode streams with pH equalization; phosphorus removal/recovery (e.g., Fe/Al coagulation or, where conditions allow, struvite crystallization) [46]; ammonia removal/recovery (e.g., air stripping with acid scrubbing, membrane contactors, or ion exchange) [47]; followed by solids separation and polishing prior to co-treatment at the municipal wastewater treatment plant where permitted. This provides a practical link from bench-scale handling to application at scale.

5. Conclusions

Porewater drainage through EKG can effectively reduce the content and release flux of sediment nutrients. When the electric field was applied, sediment TN and TP were drained mainly in the form of NH_4^+-N and SRP, respectively. EKG drainage affected the release of nitrogen and phosphorus differently. NH_4^+-N in the porewater was drained much more easily than SRP, which resulted in a significant decrease in the TN/TP ratio in the overlying water. The most effective voltage gradients for restricting the release flux of TN and TP through porewater drainage were 0.5 and 1.0 V/cm, respectively. For both nitrogen and phosphorus, porewater drainage reduced release and led to periods consistent with net uptake, thereby limiting nutrient increases in the overlying water under the tested conditions. Physical processes, including porewater renewal and drainage as well as sediment pore compression, served as the key mechanisms for restricting the release of sediment nitrogen and phosphorus. Porewater drainage through EKG promoted the oxidation and remediation of the surface sediment, and most of the NH_4^+-N and SRP was drained in the first month, suggesting the potential to shorten the duration of eutrophic water remediation using EKG. Moreover, EKG drainage did not show significant negative impacts on the sediment microbial community.

Porewater drainage through EKG merely affected sediment microorganism in terms of both species and abundance. A voltage gradient of 1.0 V/cm however led to a non-significant decrease in the Chao1 index and ACE. Microorganisms play an irreplaceable role in the biogeochemical cycle of sediment nutrients. Therefore, the effects of porewater drainage through EKG on microbial enzyme activity require further detailed investigation. Furthermore, porewater drainage through EKG generates low-volume effluents with high TN and TP concentrations, and such effluents also contain other soluble cations and anions, such as Ca^{2+}, Fe^{2+}, Mg^{2+}, and Cl^{-}. Therefore, the treatment of effluents should be considered before drainage.

Supplementary Materials

The additional data and information can be downloaded at: https://media.sciltp.com/articles/others/26011215 39100834/RE-2508000026-Supplementary-Materials.pdf. Figure S1: Variations in pH, DO, and EC in overlying water in different experimental groups. Figure S2: Variations in NH_4^+-N/TN, SRP/TP, and TN/TP ratios in overlying water in representative groups. Figure S3: Relative abundance of phyla in microbial communities in sediments after different treatments. Figure S4: Variations in cathode effluent NH_4^+-N and anode effluent SRP concentrations in representative experimental groups. Figure S5: Comparison of anode (green) and cathode (red) effluent pH and EC in different experimental groups.

Author Contributions

T.X.: conceptualization, writing—reviewing and editing, supervision; L.R.: methodology, data curation, writing—original draft preparation; H.Y.: methodology, data curation; W.D.: writing—reviewing and editing; G.J.: visualization, methodology; W.Z.: methodology. All authors have read and agreed to the published version of the manuscript.

Funding

This study was funded by National Key Research and Development Program of China (2022YFC3201902), Hubei Provincial Natural Science Foundation Project (2024AFD349, 2023AFB090), Central Public Interest Scientific Institution Basal Research Fund (CKSF2025164/SH), and National Natural Science Foundation of China (51979006, 42507640).

Institutional Review Board Statement

Not applicable.

Informed Consent Statement

Not applicable.

Data Availability Statement

Data will be made available on request.

Conflicts of Interest

The authors declare no conflict of interest.

Use of AI and AI-Assisted Technologies

No AI tools were utilized for this paper.

References

1. Smith, V.H.; Schindler, D.W. Eutrophication Science: Where Do We Go from Here? *Trends Ecol. Evol.* **2009**, *24*, 201–207.
2. Zamparas, M.; Zacharias, I. Restoration of Eutrophic Freshwater by Managing Internal Nutrient Loads. A Review. *Sci. Total Environ.* **2014**, *496*, 551–562.
3. Yang, C.; Li, J.; Yin, H. Phosphorus Internal Loading and Sediment Diagenesis in a Large Eutrophic Lake (Lake Chaohu, China). *Environ. Pollut.* **2022**, *292*, 118471.
4. Yin, H.; Zhang, M.; Yin, P.; et al. Characterization of Internal Phosphorus Loading in the Sediment of a Large Eutrophic Lake (Lake Taihu, China). *Water Res.* **2022**, *225*, 119125.

5. Tang, X.; Li, Q.; Wang, Z.; et al. *In Situ* Electrokinetic Isolation of Cadmium from Paddy Soil through Porewater Drainage: Effects of Voltage Gradient and Soil Moisture. *Chem. Eng. J.* **2018**, *337*, 210–219.
6. Fan, X.; Gao, S.; Zhang, Y.; et al. Stimulation of High-Concentration Dissolved Nitrogen and Reactive Phosphorus in Lake Taihu Sediments on the Initiation and Maintenance of Cyanobacterial Blooms. *Sci. Total Environ.* **2022**, *851*, 158088.
7. Jiang, H.; Wang, C.; Bai, L.; et al. Advances and Prospects in Lake Environment Science and Engineering: A Review. *J. Lake Sci.* **2020**, *32*, 1278–1296.
8. Yang, C.; Yang, P.; Yin, H. *In Situ* Control of Internal Nutrient Loading and Fluxes in the Confluence Area of an Eutrophic Lake with Combined P Inactivation Agents and Modified Zeolite. *Sci. Total Environ.* **2021**, *775*, 145745.
9. Yin, H.; Douglas, G.B.; Cai, Y.; et al. Remediation of Internal Phosphorus Loads with Modified Clays, Influence of Fluvial Suspended Particulate Matter and Response of the Benthic Macroinvertebrate Community. *Sci. Total Environ.* **2018**, *610*, 101–110.
10. Han, H.; Li, Z. Effects of Macrophyte-Associated Nitrogen Cycling Bacteria on ANAMMOX and Denitrification in River Sediments in the Taihu Lake Region of China. *Ecol. Eng.* **2016**, *93*, 82–90.
11. Wen, D.; Fu, R.; Li, Q. Removal of Inorganic Contaminants in Soil by Electrokinetic Remediation Technologies: A Review. *J. Hazard. Mater.* **2021**, *401*, 123345.
12. Han, D.; Wu, X.; Li, R.; et al. Critical Review of Electro-Kinetic Remediation of Contaminated Soils and Sediments: Mechanisms, Performances and Technologies. *Water Air Soil Pollut.* **2021**, *232*, 335.
13. Shin, S.-Y.; Park, S.-M.; Kitae, B. Soil Moisture Could Enhance Electrokinetic Remediation of Arsenic-Contaminated Soil. *Environ. Sci. Pollut. Res.* **2017**, *24*, 9820–9825.
14. Choi, J.-H.; Maruthamuthu, S.; Lee, H.-G.; et al. Removal of Phosphate from Agricultural Soil by Electrokinetic Remediation with Iron Electrode. *J. Appl. Electrochem.* **2010**, *40*, 1101–1111.
15. Weigand, H.; Marb, C.; Weiss, W.; et al. Electrokinetic Phosphorus Recovery from Packed Beds of Sewage Sludge Ash: Yield and Energy Demand. *J. Appl. Electrochem.* **2010**, *40*, 1069–1078.
16. Ghaeminia, M.; Mokhtarani, N. Remediation of Nitrate-Contaminated Groundwater by PRB-Electrokinetic Integrated Process. *J. Environ. Manag.* **2018**, *222*, 234–241.
17. Liu, R.; Wang, H.; Liu, Z.; et al. Electrokinetic Remediation with Solar Powered for Electrolytic Manganese Residue and Researching on Migration of Ammonia Nitrogen and Manganese. *J. Water Process Eng.* **2020**, *38*, 101655.
18. Li, S.; Zheng, C.; Yang, S.; et al. Reduction of Nitrogen and Phosphorus Loading from Polluted Sediment by Electrolysis. *Ecol. Eng.* **2021**, *159*, 106088.
19. Wang, D.; Tang, X.; Li, R.; et al. Electrokinetic Geosynthetics Restrained Nitrogen Release from Sediment to Overlying Water through Porewater Drainage. *Chemosphere* **2022**, *307*, 135674.
20. Tang, X.; Li, R.; Han, D.; et al. Impacts of Electrokinetic Isolation of Phosphorus through Porewater Drainage on Sediment Phosphorus Storage Dynamics. *Environ. Pollut.* **2020**, *266*, 115210.
21. Wu, X.; Li, R.; Tang, X.; et al. Performance of Separating Sediment Endogenous Nitrogen via Electrokinetic Drainage of Porewater. *China Environ. Sci.* **2021**, *41*, 1208–1218.
22. Pardo, P.; Rauret, G.; López-Sánchez, J.F. Shortened Screening Method for Phosphorus Fractionation in Sediments A Complementary Approach to the Standards, Measurements and Testing Harmonised Protocol. *Anal. Chim. Acta* **2004**, *508*, 201–206.
23. Yin, H.; Yang, C.; Yang, P.; et al. Contrasting Effects and Mode of Dredging and *In Situ* Adsorbent Amendment for the Control of Sediment Internal Phosphorus Loading in Eutrophic Lakes. *Water Res.* **2021**, *189*, 116644.
24. Wang, Z.; Wang, C.; Jiang, H.; et al. Higher Dissolved Oxygen Levels Promote Downward Migration of Phosphorus in the Sediment Profile: Implications for Lake Restoration. *Chemosphere* **2022**, *301*, 134705.
25. Hopkinson, C.S.; Giblin, A.E.; Tucker, J.; et al. Benthic Metabolism and Nutrient Cycling along an Estuarine Salinity Gradient. *Estuaries* **1999**, *22*, 863–881.
26. Beutel, M.W. Inhibition of Ammonia Release from Anoxic Profundal Sediments in Lakes Using Hypolimnetic Oxygenation. *Ecol. Eng.* **2006**, *28*, 271–279.
27. Reyter, D.; Bélanger, D.; Roué, L. Nitrate Removal by a Paired Electrolysis on Copper and Ti/IrO_2 Coupled Electrodes-Influence of the Anode/Cathode Surface Area Ratio. *Water Res.* **2010**, *44*, 1918–1926.
28. Chauhan, R.; Srivastava, V.C. Superior Reduction of Nitrate with Simultaneous Oxidation of Intermediates and Enhanced Nitrogen Gas Selectivity via Novel Electrochemical Treatment. *Process Saf. Environ. Prot.* **2021**, *147*, 245–258.
29. Weber, K.A.; Achenbach, L.A.; Coates, J.D. Microorganisms Pumping Iron: Anaerobic Microbial Iron Oxidation and Reduction. *Nat. Rev. Microbiol.* **2006**, *4*, 752–764.
30. Ma, S.; Wang, H.; Wang, H.; et al. High Ammonium Loading Can Increase Alkaline Phosphatase Activity and Promote Sediment Phosphorus Release: A Two-Month Mesocosm Experiment. *Water Res.* **2018**, *145*, 388–397.

31. Zhao, X.; Tan, X.; Yang, L.; et al. Cultivation of *Chlorella pyrenoidosa* in Anaerobic Wastewater: The Coupled Effects of Ammonium, Temperature and pH Conditions on Lipids Compositions. *Bioresour. Technol.* **2019**, *284*, 90–97.
32. Yang, D.; Chen, Q.; Liu, R.; et al. Ammonia Recovery from Anaerobic Digestate: State of the Art, Challenges and Prospects. *Bioresour. Technol.* **2022**, *363*, 127957.
33. Kissel, D.E. *Encyclopedia of Soils in the Environment*; Elsevier: Amsterdam, The Netherlands, 2005; pp. 56–64.
34. Kim, W.-S.; Jeon, E.-K.; Jung, J.-M.; et al. Field Application of Electrokinetic Remediation for Multi-Metal Contaminated Paddy Soil Using Two-Dimensional Electrode Configuration. *Environ. Sci. Pollut. Res.* **2014**, *21*, 4482–4491.
35. Kim, K.-W.; Kim, Y.-J.; Kim, I.-T.; et al. Electrochemical Conversion Characteristics of Ammonia to Nitrogen. *Water Res.* **2006**, *40*, 1431–1441.
36. Urban, N.R.; Dinkel, C.; Wehrli, B. Solute Transfer across the Sediment Surface of a Eutrophic Lake: I. Porewater Profiles from Dialysis Samplers. *Aquat. Sci.* **1997**, *59*, 1–25.
37. Dong, M.; Nielsen, L.; Yang, S.; et al. Cable Bacteria: Widespread Filamentous Electroactive Microorganisms Protecting Environments. *Trends Microbiol.* **2024**, *32*, 697–706.
38. Guedes, P.; Dionisio, J.; Couto, N.; et al. Electro-Bioremediation of a Mixture of Structurally Different Contaminants of Emerging Concern: Uncovering Electrokinetic Contribution. *J. Hazard. Mater.* **2021**, *406*, 124304.
39. Shi, Y.; Wei, Z.; Xu, Y.; et al. Effects of Electrochemical Intervention on the Remediation of Black-Odorous Water: Insights into Microbial Community Dynamics and Functional Shifts in Sediments. *Water Sci. Technol.* **2023**, *87*, 2776–2792.
40. Mena, E.; Villaseñor, J.; Cañizares, P.; et al. Effect of a Direct Electric Current on the Activity of a Hydrocarbon-Degrading Microorganism Culture Used as the Flushing Liquid in Soil Remediation Processes. *Sep. Purif. Technol.* **2014**, *124*, 217–223.
41. Li, F.; Guo, S.; Wang, S.; et al. Changes of Microbial Community and Activity under Different Electric Fields during Electro-Bioremediation of PAH-Contaminated Soil. *Chemosphere* **2020**, *254*, 126880.
42. Xu, H.; Zhu, Y.; Du, M.; et al. Subcellular Mechanism of Microbial Inactivation during Water Disinfection by Cold Atmospheric-Pressure Plasma. *Water Res.* **2021**, *188*, 1165123.
43. Tucci, M.; Viggi, C.; Nunez, A.; et al. Empowering Electroactive Microorganisms for Soil Remediation: Challenges in the Bioelectrochemical Removal of Petroleum Hydrocarbons. *Chem. Eng. J.* **2021**, *419*, 130008.
44. Duncan, S.; Louis, P.; Thomson, J.; et al. The Role of pH in Determining the Species Composition of the Human Colonic Microbiota. *Environ. Microbiol.* **2009**, *11*, 2112–2122.
45. Hemkemeyer, M.; Schwalb, S.; Heinze, S.; et al. Functions of Elements in Soil Microorganisms. *Microbiol. Res.* **2021**, *252*, 126832.
46. Luo, G. Review of Waste Phosphorus from Aquaculture: Source, Removal and Recovery. *Rev. Aquac.* **2022**, *15*, 1058–1082.
47. Kar, S.; Singh, R.; Gurian, P.; et al. Life Cycle Assessment and Techno-Economic Analysis of Nitrogen Recovery by Ammonia Air-Stripping from Wastewater Treatment. *Sci. Total Environ.* **2023**, *857*, 159499.